Citation: Biswa Ranjan Swain and Ashish Kumar Sharma.Investigation of frequency and polarization tunable monopole antenna for 5G-enabled smart street networks. *Journal of Harbin Institute of Technology (New Series)*. DOI: 10.11916/j.issn.1005-9113.2025098

Investigation of Frequency and Polarization Tunable Monopole Antenna for 5G-Enabled Smart Street Networks

*Biswa Ranjan Swain and Ashish Kumar Sharma**

(*Department of Electronics and Telecommunication Engineering, Veer Surendra Sai University of Technology, Burla 768018, India*)

Abstract: In this article, a frequency and polarization tunable antenna is designed and prototyped for TDD B40, TDD NR N41, and N78 band 5G advanced communications. Frequency and polarization tunable properties are achieved here by adding five SMP1345-079LF PIN diodes at different locations of the radiating patch and by optimizing the structure. At first, the antenna is designed in HFSS and then it is evaluated under various atmospheric circumstances through MATLAB simulation based environment in existence with foliage and rain. Even with atmospheric losses, the antenna can maintain a descent received power level below −100 dB, making it well-suited for next generation wireless applications. The designed antenna resonates at 2.3, 2.5, 3.5, and 5.5 GHz with PIN diode ON/OFF conditions. The key challenge here is to design a reconfigurable antenna with tunable capabilities to operate across major LTE/NR bands, including 5.5 GHz Wi-Fi, in both on and off conditions, and to validate it in real-world scenarios with multiple environmental factors. The proposed antenna and its array with balanced performance characteristics and beam steering capabilities are found to be an appropriate candidate for outdoor smart street advanced 5G communications.

Keywords: 5G-NR; reconfigurable patch antennas; PIN diode; TDD B40 band; TDD N41 band; N78 band

CLC number: TN82 **Document code**: A **Article ID**: 1005-9113(2026)00-0000-13

0 Introduction

Nowadays, radio communication platforms need high spectral capacity to fulfil the necessity of broadband based IoT devices, data analysis and smart phones. Along with the existing spectrum in the sub 6 GHz band, more bands are needed for these 5G services. To address these challenges, the telecom service provider needs more operating bands for the upcoming advanced 5G. Currently, N78 is the most popular band used in 5G communication worldwide. This band is well known for its advantage for providing capacity in dense urban areas. However, in less dense urban areas and sub-urban areas, the N78 band is achieving less success due to its limited coverage. Hence, considering all these, another NR band N41 is now proposed for advanced 5G communication. This band provides a better balance between coverage and capacity in sub-urban areas. This band uses TDD technology to achieve high-speed, low-latency communication with wide coverage, with a comparatively higher operating wavelength than the N78 band. The addition of the N41 band for cutting-edge 5G applications will improve the data communication network's efficiency, as well as its business prospects in the future. Similarly, for LTE private networks, B40 with TDD technology plays a vital role in high bandwidth data transfer among wireless devices, offering better range than the N41 and N78 bands.

5G Fixed Wireless Access (FWA) is rapidly adopted nowadays for indoor wireless communications. This study proposes outdoor smart street applications for 5G FWA technology in high-capacity hotspot zones. The key requirements for antennas in 5G enabled smart street networks are wideband/multiband operation, compact/low-profile design, high gain capability, environmental robustness, low latency, and energy efficient solutions[1]. The antenna should support multiple bands for carrier aggregation too. Similarly, it should be designed for smooth integration into street infrastructure, such as lamp posts, traffic lights, and CCTV poles with the capacity to withstand

Received 2025-08-07.

* Corresponding author. Ashish Kumar Sharma, Ph.D., Assistant professor. Email: biswa.iitkgp.ece@gmail.com, ashishksharma29@gmail.com.

outdoor temperatures, rain, dust, etc. In indoor FWA systems, two antennas are used, one to communicate with nearby existing 5G base stations, and the other to connect to user devices via Wi-Fi. To minimize the use of two different antennas, a single frequency reconfigurable antenna is proposed for both communication with nearby base stations and with user devices on the street. For this scenario, multiband antennas can be used, but they are very sensitive and less resistant to harmonic frequencies. So, there will be a chance for interference with other harmonic frequencies. The main reason to choose a resonator structure over a wideband structure for the same frequency range is to avoid interference with other existing applications within that range. Another main reason is that the resonator structure always has stable radiation characteristics, consistent gain, low noise, and limited interference with adjacent channels compared to wideband designs. Also, it is quite difficult to design a multiband antenna for their use in different bands other than harmonics. Hence, considering all the above points, frequency reconfigurable antennas are found to be suitable candidates for the purpose than multiband/wideband antennas. The choice of perfect Tx and Rx antennas defines the strength of a network, which is purely based on them for high-speed, reliable, and low-latency communications.The microstrip patch antenna, with low cost and low profile, is in high demand among researchers for its compactness, consistency, and effectiveness. The conventional multiband MPAs still need proper design and band stop filters to be highly resistant to their resonant harmonic frequencies to avoid inter frequency interference. Numerous techniques have already been investigated in the literature to achieve multi-frequency operation of antennas. Some approaches use shorting[2], inductively loaded cuboid ridges[3], fractal geometries[4], topology-driven configurations[5], integration of meta-materials[6-7], and split-ring resonator structures [8-11] in microstrip antennas. In 2012, Split-Ring Resonators (SRRs) were deployed on metasurfaces to design multiband microstrip antennas[7]. The antenna exhibits multiple resonant bands, but its performance is significantly affected by lower gain. The researchers achieved 3 operational bands for a fractal patch by varying its iterations and indentations[4-5], resulting in increased volume. Even though in Refs.[2] and [3], the antennas exhibit multiple resonating frequencies through the cuboid ridge, with reduced operating bands. DGS is also an effective methodology for developing compact multiband patch antennas[12-14]. Many structures, such as dumbbells[12], circular strips[13], triangular shapes[14], etc., have been investigated for miniaturized patch designs. In Ref.[15], a genetic algorithm is applied to design compact microstrip antennas. Among other concepts, antenna frequency reconfigurability by the addition of switch diodes is also an effective process. Antenna resonant frequencies can be shifted by switching these diodes on and off. In addition, the proposed antenna exhibits other resonant frequencies due to single-directional current flow and the diode's blocking properties.

In this article, a frequency and polarization tunable antenna is developed for TDD B40, TDD NR N41, and N78-band 5G advanced communications. Future 5G communication also needs higher data rates to handle large data transfers for various low-latency applications. Increasing the number of antenna elements can help achieve a higher modulation order, thus increasing the data rate. However, the frequency-tuning capability of the proposed antenna from TDD B40 to N41 and N78 bands, with higher bandwidth can help to achieve higher data rate in short range smart street communications. In addition, the proposed antenna element can be modified into a MIMO array to enhance data rate by simultaneously transmitting or receiving multiple data streams using spatial multiplexing. Here, frequency and polarization reconfigurations are achieved through five SMP1345-079LF PIN diodes at different locations on the radiating patch, optimizing the structure. The proposed circularly polarized antenna has the advantage of reducing the harmful effects of multipath propagation, being insensitive to the orientation of transmitter and receiver, and having strong anti-interference capabilities. Similarly, an antenna with circular polarization can reduce path loss and enable a reliable, robust network for communication among devices. First, a reconfigurable microstrip antenna is designed and optimized in HFSS, and it is evaluated in MATLAB for various atmospheric environments in a 5G smart street application, in the presence of different amounts of foliage and rain.

Initially, an edge fed dual band patch is considered for 2.3 GHz and 5.5 GHz. In the next step, 5 PIN diodes are added to achieve frequency

tunability of the patch in Section 1. Then, the prototype of the proposed antenna is fabricated in Section 2, where the simulation and measured results are matched. Then, in Section 3, the antenna is tested in a MATLAB real-time simulation environment, considering different amounts of rain and foliage for 5G smart street communications. After comparing the proposed design with available similar designs, Section 4 concludes our investigation toward a frequency- and polarization-tunable antenna for smart street applications.

1 Frequency and Polarization Tunable Antenna Design

The major objective of this work is to create a high gain, directive frequency tunable antenna for 5G smart street applications. Hence, a simple, miniaturized dual-frequency antenna design is considered first. This compact, broadband antenna features a two-strip monopole for low-band operation and a planar monopole for high-band operation. This compact two-strip monopole antenna design is inspired by the work presented in Ref.[16], specifically redesigned for 5G smart street applications. However, to make the antenna suitable for advanced 5G smart street communication, five PIN diodes are added at different positions, and the structure is physically optimized in ANSYS HFSS using its array. The patch antenna comprises a T-strip on the front side and S-strip on the back side of the substrate. The two-strip monopole is intended to operate at the lower band; in addition, a planar monopole with a T-strip section is added for operation at the higher band. In this design, the T-strip is positioned within an area enclosed by the upper section of the S-strip, with its lower section overlapping the lower section of the S-strip. Here the planar monopole and T-strip sections are fed by a single 50 Ω microstrip feed, whereas the S-strip is connected to the ground plane.

The structural configuration of the proposed patch antenna is shown in Fig.1, while its detailed design parameters are listed in Table 1. RT Duroid 5880 with dielectric constant (εr) of 2.2 is taken as a dielectric substrate with a thickness of 0.254 mm. Then, an SMP1345-079LF PIN diode is positioned at the feed joint to enable frequency tunability of the antenna.

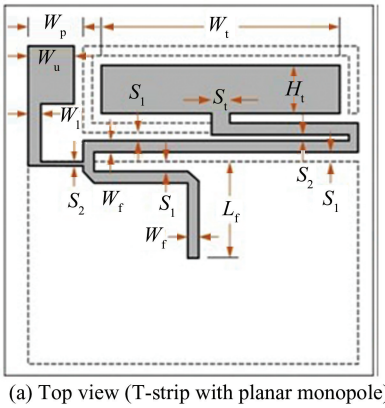

(a) Top view (T-strip with planar monopole)

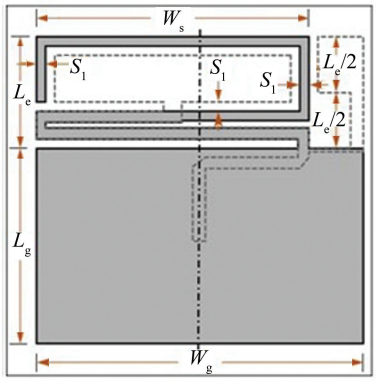

(b) Back View (S-strip)

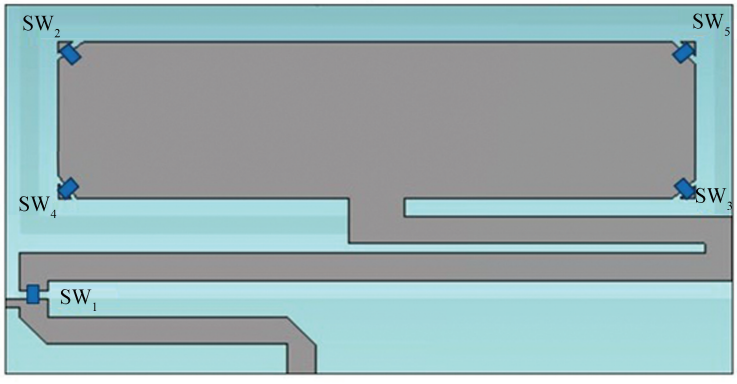

(c) Switch position for frequency and polarization reconfiguration

Fig.1 Antenna design: top view, back view, and switch position for frequency and polarization reconfiguration

In the suggested design, both the T-strip and the planar monopole are fed by a 50 Ω microstrip line, and the lower S-strip is terminated at the ground plane. By adding a switchable PIN diode to the feed of the T-strip, it adjusts the feed electrical length and alternately adjusts the input resistance to the design to maintain impedance near 50 Ω across multiple reconfigurable states. For the SW_1-ON condition, the planar monopole is designed to operate at the higher band, while the T- and S-stripes are designed to operate at the lower band, maintaining impedance matching by length tuning. In the SW_1-OFF condition, the disturbance in the surface current between the T-strip and S-strip helps generate the additional 3.5 GHz band while stabilizing the other two primary bands. Finally, another 4 same PIN diodes are placed at the corner edges to achieve polarization tunability.

Table 1 Antenna physical parameters (mm)

L_g	W_f	L_f	S_1	S_2	E_r	H	S_t	W_t	H_t
60	0.75	15	0.5	0.5	2.2	0.254	1.5	16.78	4.25
W_s	W_p	W_u	W_1	W_g	L_e	*X*-total	*Y*-total	*Z*-total	
19	3.96	3.5	0.5	22.96	8	22.96	68	0.254	

A total of five (SW_1-SW_5) PIN diodes are fitted on the feeding line connecting to the planar monopole and the edge of the T-strip patch to achieve frequency and polarization reconfiguration, respectively. Figs. 2 (a) and (b) depict the equivalent electrical circuits of a pin diode in forward bias (ON) and reverse bias (OFF) configurations, respectively. The parameter values of the RLC component of the SMP1345-079LF PIN diode in the ON and OFF configurations are used in the ANSYS HFSS simulation, as shown in Table 2.

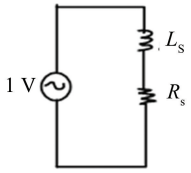

(a)The equivalent configuration of a PIN diode in the forward bias

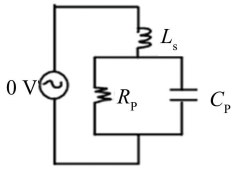

(b) The equivalent configuration of a PIN diode in the reverse bias

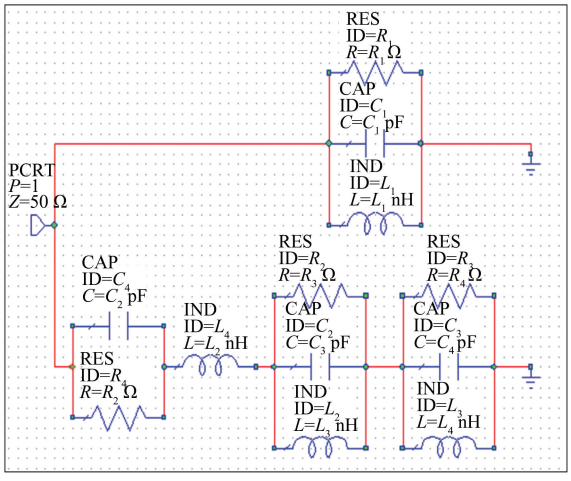

(c) SW_1-off

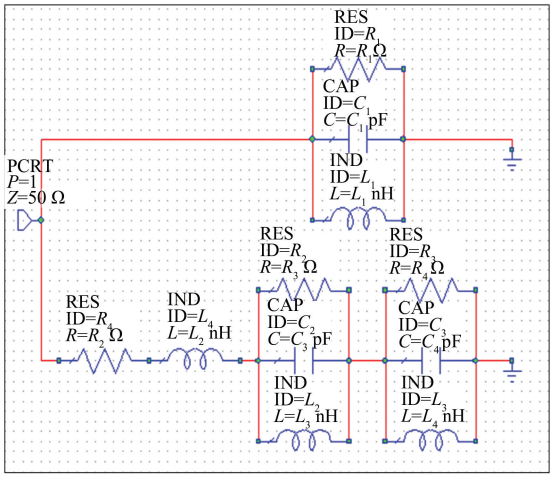

(d) SW_1-on

Fig.2 Electrical schematic illustrating the equivalent configuration of a PIN diode (a) the forward bias (ON state) and (b) the reverse bias (OFF state) switching modes and Equivalent Electrical Circuit Model of the proposed design (c) SW_1-OFF, (d) SW_1-ON state

Table 2 Parametric values of RLC components

Switching state	RLC parameters			
	RS (MΩ)	RP (KΩ)	LS (nH)	CP (pF)
ON	3.5	–	0.45	–
OFF	–	3.5	0.45	1.2

In the forward-bias condition, the equivalent circuit of a PIN diode is shown as a series combination of an inductance (L_S) and a low series resistance (R_S). Conversely, in the reverse-bias condition, the equivalent circuit consists of a parallel

combination of resistance (RP) and capacitance (CP), in series with an inductance (L_S). A single PIN diode switch (SW_1) is added to achieve frequency reconfiguration. Similarly, four diode switches SW_2-SW_5 are used at the T-strip patch edge to achieve polarization reconfiguration. The different switching cases observed for hybrid tunability are shown in Table 3. The equivalent circuit model for the proposed antenna design is depicted in Fig.2 for both SW_1 ON and OFF conditions. The equivalent circuit contains three parallel R-L-C sections connected in series with a 50 Ω transmission line at the start and a ground at the end. Each upper R-L-C section is responsible for the higher resonating frequency, whereas the lower two parallel R-L-C sections are responsible for the T-strip at the patch and S-strip at the ground plane. These two combined result in lower resonant frequencies. For SW_1 ON/OFF conditions, an additional R-L-C circuit is added as shown in Fig.2. For SW_1 OFF condition, a parallel R-C is connected in series with L and for SW_1 ON condition, a series R-L circuit is established as per the properties of SMP1345-079LF PIN diode. Both circuits are connected between the 50 Ω line and the lower two parallel R-L-C circuits for ON/OFF conditions, separately. From the parameters, L and C affect the bandwidth and the resonant frequency. Similarly, R helps determine the S11 match at each frequency. This way, all the circuit parameters are varied to get an exact match with the simulated design.

Table 3 Switching cases observed for hybrid tunability

Switching cases	Switches	Tunability mechanism	Results
Case-1	SW_1-ON	Frequency tunability	Resonating bands: 2.3/5.5 GHz
Case-2	SW_1-OFF	Frequency tunability	Resonating bands: 2.5/3.5/5.5 GHz
Case-3	SW_1-ON, SW_2, SW_3, SW_4, SW_5-ON	Polarization tunability	Linear polarization
Case-4	SW_1-OFF, SW_2, SW_3-OFF, SW_4, SW_5-ON	Polarization tunability	Left hand circular polarization
Case-5	SW_1-OFF, SW_2, SW_3-ON, SW_4, SW_5-OFF	Polarization tunability	Right hand circular polarization

For Case-1, when SW_1 is ON, it allows the current to flow through both patches, resulting in resonance in the TDD B40 2.3 GHz band and the Wi-Fi 5.5 GHz band. During SW_1 OFF condition, the current flow is disturbed, helping the same antenna resonate at 3 different frequencies: TDD NR N41 2.5 GHz, N78 3.5 GHz, and Wi-Fi 5.5 GHz. These frequency reconfigurability scenarios are analyzed in Fig. 3(a). Further, in the next case, all four switches SW_2-SW_5 are in ON condition, which helps the antenna to radiate with linear polarization. While SW_2, SW_3 are in OFF condition and SW_4, SW_5 are in ON condition, Left Hand Circular Polarization (LHCP) and with SW_2, SW_3 as ON and SW_4, SW_5 as OFF condition, Right Hand Circular Polarization (RHCP) is observed at 3.5 GHz, as shown in Fig.3 (b).

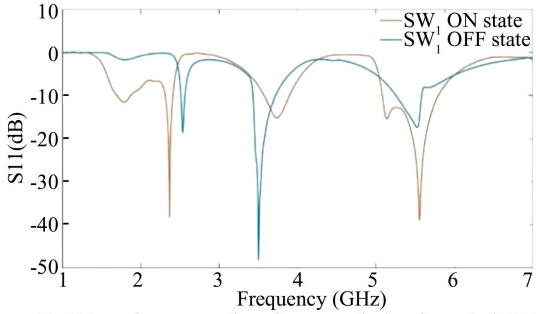

(a) S11 vs. frequency plot of antenna design for switch SW_1 ON/OFF configuration

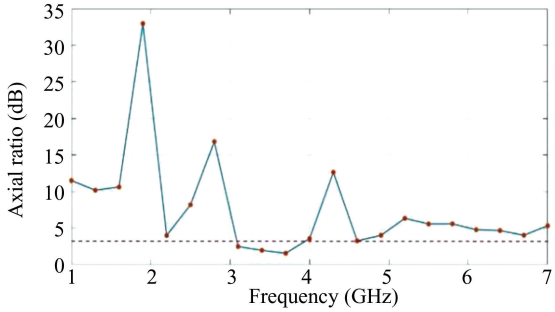

(b) Axial ratio vs. frequency for the proposed antenna

Fig.3 S11 vs. frequency plot of antenna design for Switch SW_1 ON/OFF configuration and axial ratio vs. frequency for the proposed antenna

The surface current distribution plots for the proposed design are shown in Fig. 4 for different switching conditions. Here, it is seen that the surface currents are altered by introducing perturbations at the patch with the ON/OFF condition of switches, producing a multiband resonance.

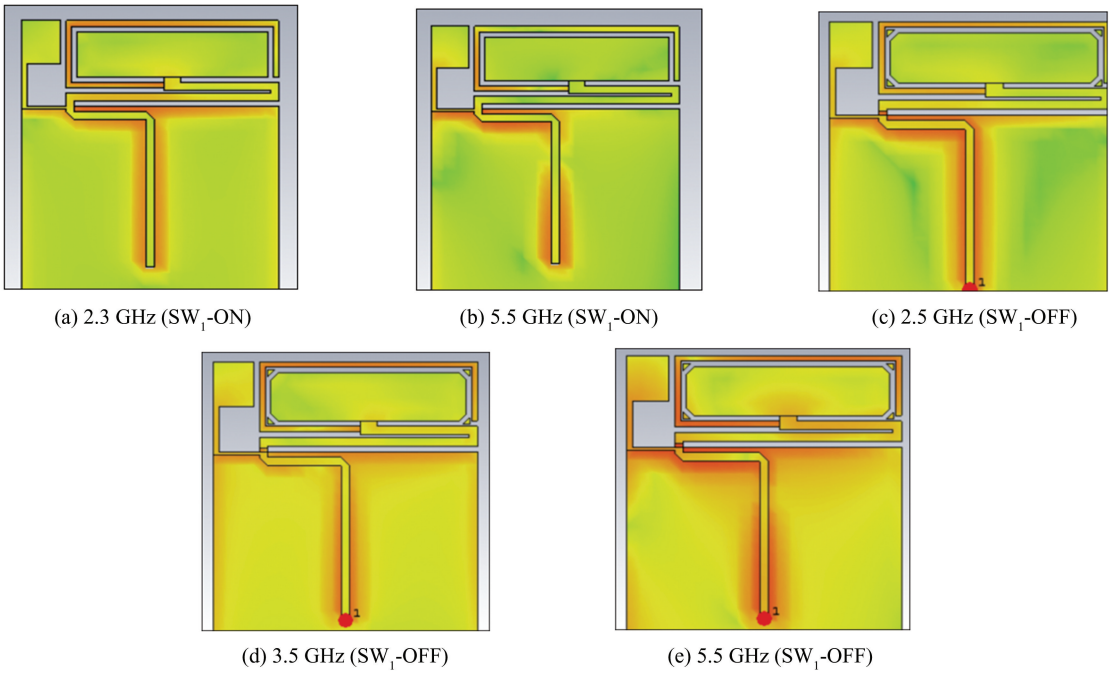

(a) 2.3 GHz (SW_1-ON) (b) 5.5 GHz (SW_1-ON) (c) 2.5 GHz (SW_1-OFF)

(d) 3.5 GHz (SW_1-OFF) (e) 5.5 GHz (SW_1-OFF)

Fig.4 Surface current visualization of 2.3 GHz (SW_1-ON), 5.5 GHz (SW_1-ON), 2.5 GHz (SW_1-OFF), 3.5 GHz (SW_1-OFF), and 5.5 GHz (SW_1-OFF)

2 Results and Discussions

Now, this proposed antenna design is fabricated on the same RT Duroid 5880 substrate. The S11 and other reflection characteristics are measured using an Agilent N5247A VNA and matched to the simulated results. The miniaturized antenna has a dimension of 63 mm×8 mm, as shown in Fig.5. Here the fabricated prototype is in connection with the VNA for reflection and radiation characteristics measurements. Fig.6 portrays simulated and measured S11 results for both SW_1 ON/OFF scenarios. Here it is seen that the measured S11 curve follows the simulated S11 curves. The slight discrepancy between the simulated and measured results may be attributed to fabrication inaccuracies.

Fig.5 The prototype of the proposed antenna, along with the VNA setup and the anechoic chamber measurements, is shown with both front and back views

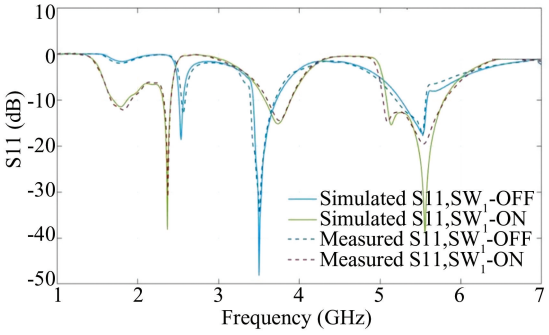

Fig.6 S11 vs. frequency plots for SW_1 ON/OFF conditions for both simulation and measurement

The fabricated design is then placed in an anechoic chamber for radiation field measurement. Fig. 5 depicts the measurement arrangements for the proposed antenna.

A horn is configured as the transmitter antenna and the reconfigurable antenna prototype is configured as the receiving antenna. The simulation and measurement radiation patterns for E-plane (*ZX*-plane, $\phi = 0°$) and H-plane (*YZ*-plane, $\phi = 90°$) are shown in Fig.7 for different switching conditions. The simulation radiation patterns exhibit good agreement with the respective measured ones. The antenna generates a symmetric directivity pattern in the E-and H-planes, with small irregularities in the gain plot due to imperfections in the microstrip patch. Similarly, the LHCP and RHCP radiation patterns at 3.5 GHz are shown in Fig. 8. Figs.9 and 10 depict the gain and radiation efficiency plots.

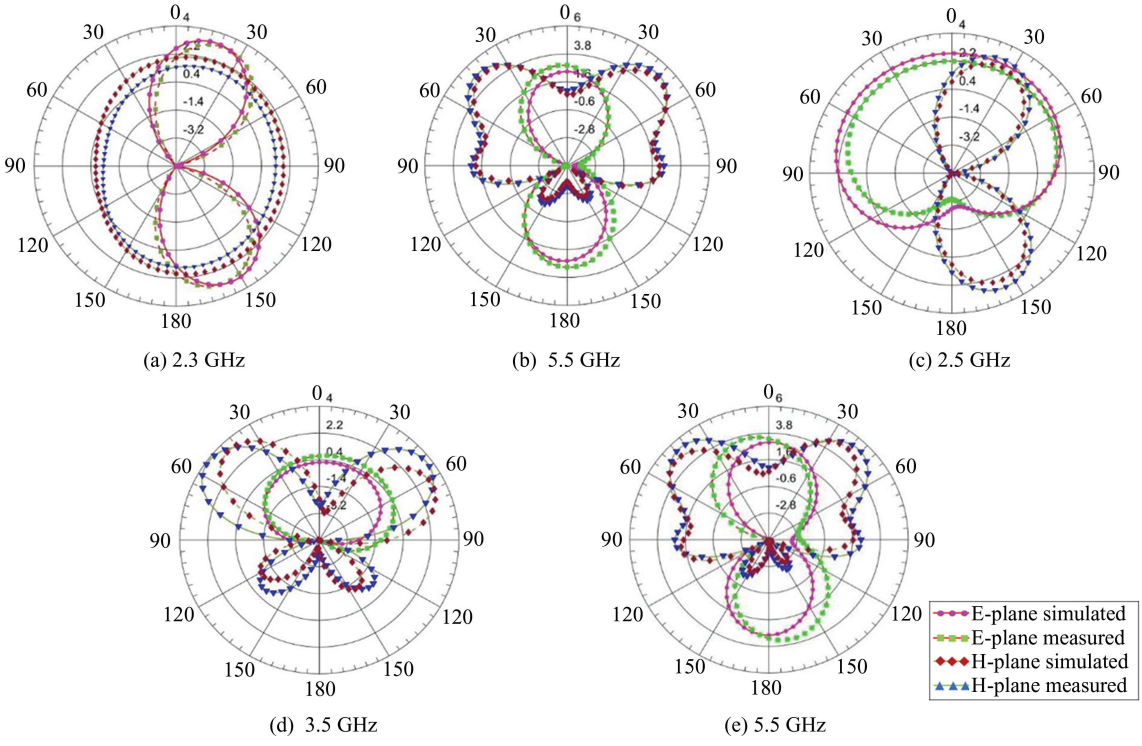

Fig.7 E-plane and H-plane radiation pattern, 2.3, 5.5, 2.5, 3.5, 5.5 GHz for different switching configuration

From the same figures, it can be clearly observed that the antenna shows a maximum gain of 6.5 dB with an overall range of 3 to 6 dB, throughout its resonant frequencies. The simulated and measured gains at all tunable frequencies are shown in Table 4 for both SW_1 ON/OFF conditions. Similarly, the antenna exhibits maximum radiation efficiency of 98% with an overall range of 75% to 95%. Once the prototype design is completed and performance matches, the design is then compared with similar antennas from the literature.

Table 4 Simulated and measured gain values for SW_1 ON/OFF conditions

Switching condition	Resonant frequency (GHz)	Simulated gain (in dBi)	Measured gain (in dBi)
SW_1-ON	2.3	3.1	3.20
	5.5	5.2	5.18
SW_1-OFF	2.5	3.1	3.20
	3.5	4.0	3.95
	5.5	5.4	5.37

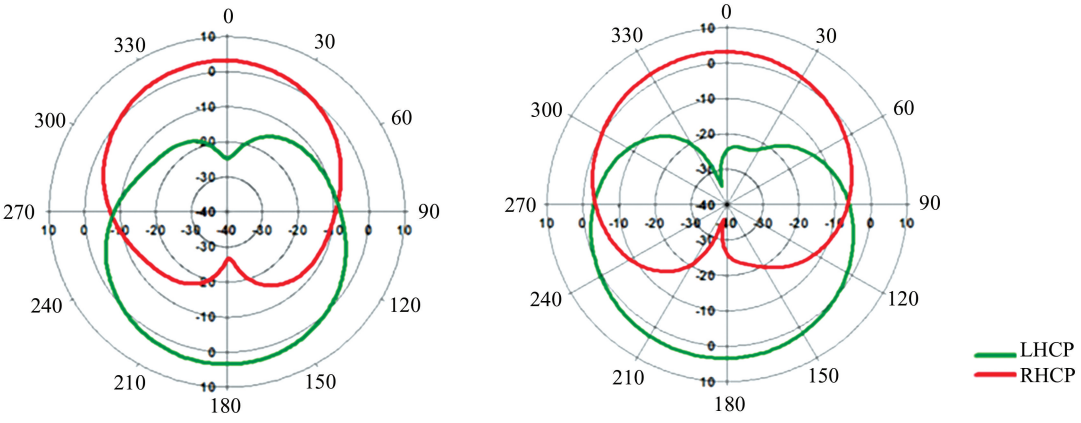

(a) ϕ =0° (b) ϕ =0°

Fig.8 LHCP and RHCP radiation pattern at 3.5 GHz in 4th and 5th switching configuration

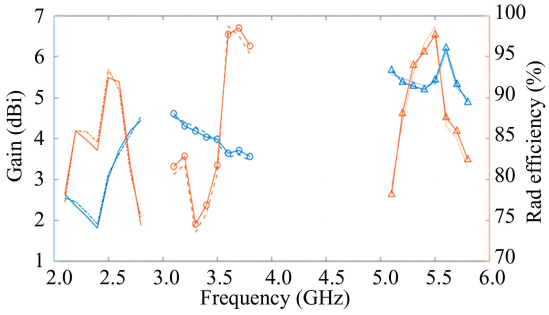

Fig.9 Gain and radiation efficiency vs. frequency for both SW_1 OFF condition (1st switching configuration)

As the antennas considered for comparison operate at different frequencies, their physical parameters are expressed in terms of wavelength to ensure a valid comparison. Other important parameters, such as impedance bandwidth, amount of size reduction, and overall gain, are also presented in Table 5 for comparison with the proposed design and other antennas. Among all the designs operating in the nearby ranges, the prototype developed in Ref.[20], show a maximum size of 0.92 λ ×0.76 λ , taken as a benchmark to estimate % of size reduction.

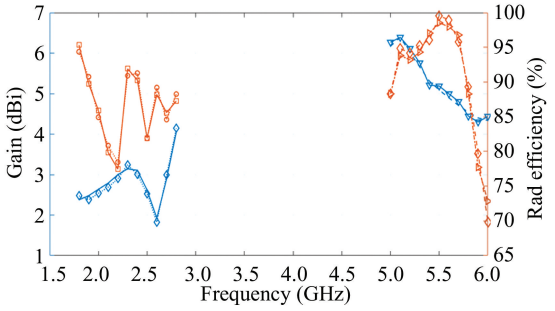

Fig.10 Gain and radiation efficiency vs. frequency for both SW_1 ON condition (2nd switching configuration)

Table 5 Performance comparison for various developed antennas

Antenna	Antenna dimension	Size reduction(%)	Operating frequency (GHz)	Gain (dB)	Bandwidth (MHz)
Ref. [17], 2022	0.48 λ ×0.40 λ	72	5.2	6.21	836
Ref. [18], 2024	0.56 λ ×0.56 λ	55	6.5	4.26	810
Ref.[19], 2017	0.46 λ ×0.49 λ	67	4.5	5.24	180
Ref.[20], 2023 (Reference)	0.92 λ ×0.76 λ	–	6.0	3.80	900
Ref.[21], 2023	0.33 λ ×0.33 λ	89	4.5	2.65	800
Ref.[22], 2023	1.89 λ ×1.50 λ	−75	16.4	10.60	9800
Ref.[23], 2024	1.04 λ ×1.04 λ	−35	26.0	4.40	8000
Ref.[24], 2024	1.87 λ ×1.87 λ	−80	28.0/38.0	7.50	3000
Proposed antenna with diode	0.52 λ ×0.17 λ	87	2.3/5.5, 2.5/3.5/5.5	5.21	380

In Ref.[21], the antenna has the smallest size compared to the slightly higher one in our case. However, the design exhibits a low gain of 2.65 dBi, compared to the proposed reconfigurable design's 5.21 dBi. The design in Ref.[17] has the maximum gain of 6.21 dB among all, but the same design still exhibits a comparatively larger dimension. Similarly, among all, the design in Ref.[20], have maximum operating bandwidth, but it is possible with its larger size. Similarly, in Refs.[22−24], mmWave antennas

are developed for wideband 5G applications. These antennas have a large impedance bandwidth, but their physical dimensions, in terms of operating wavelength, are much higher than those of the proposed antenna. Many similar antennas have been developed and fabricated in the literature. But many of them lack testing of their designs to assess their suitability for the proposed applications. Hence, the main motivation of this work is not only to design and fabricate a reconfigurable antenna for LTE, NR, and Wi-Fi bands, but also to test the performance of the designed antenna in simulation environment with a practical smart street scenario with multiple environmental factors to proof the suitability of the design based on the actual value of the signal strength at the receiver. The proposed reconfigurable design may not be the best in all respects, but it offers 87% miniaturization, a gain of 5.21 dBi, and an impedance bandwidth of 380 MHz, with good performance for 5G applications such as FWA smart street networks in high-capacity hotspot zones. Therefore, this work presents the development of a pin-diode-based reconfigurable antenna with tunable LTE TDD and NR bands, and simultaneously with the Wi-Fi band. The work not only focused on the design and fabrication of the antenna but also tested it in a simulation environment with a practical smart street scenario, including multiple environmental factors, to demonstrate the design's suitability based on the actual signal strength at the receiver. This makes it unique in comparison to other available works.

3 Performance Valuation of Antenna in Matlab

At first, the same reconfigurable design is recreated in MATLAB, and its performance is evaluated through various simulations. A custom antenna is first designed by importing S11 and 3D gain patterns from HFSS into MATLAB; the radiation patterns are then matched across both simulation platforms to confirm the design is identical. Once the matching of the radiation pattern is achieved, the antenna will be evaluated in real-time environments. The workflow diagram for testing the proposed antenna in MATLAB is shown in Fig.11. Fig.12 depicts a 3D radiation-plot comparison of the proposed design between ANSYS HFSS and MATLAB simulations.

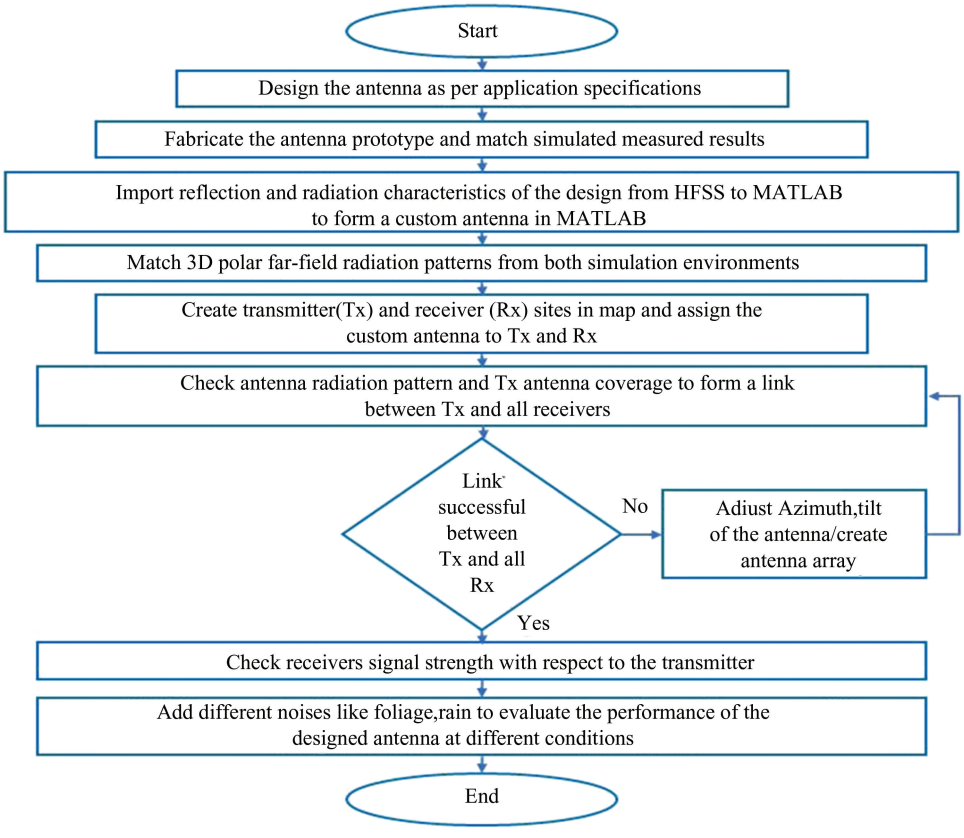

Fig.11 Process flow for the test of the proposed antenna in MATLAB simulation environments

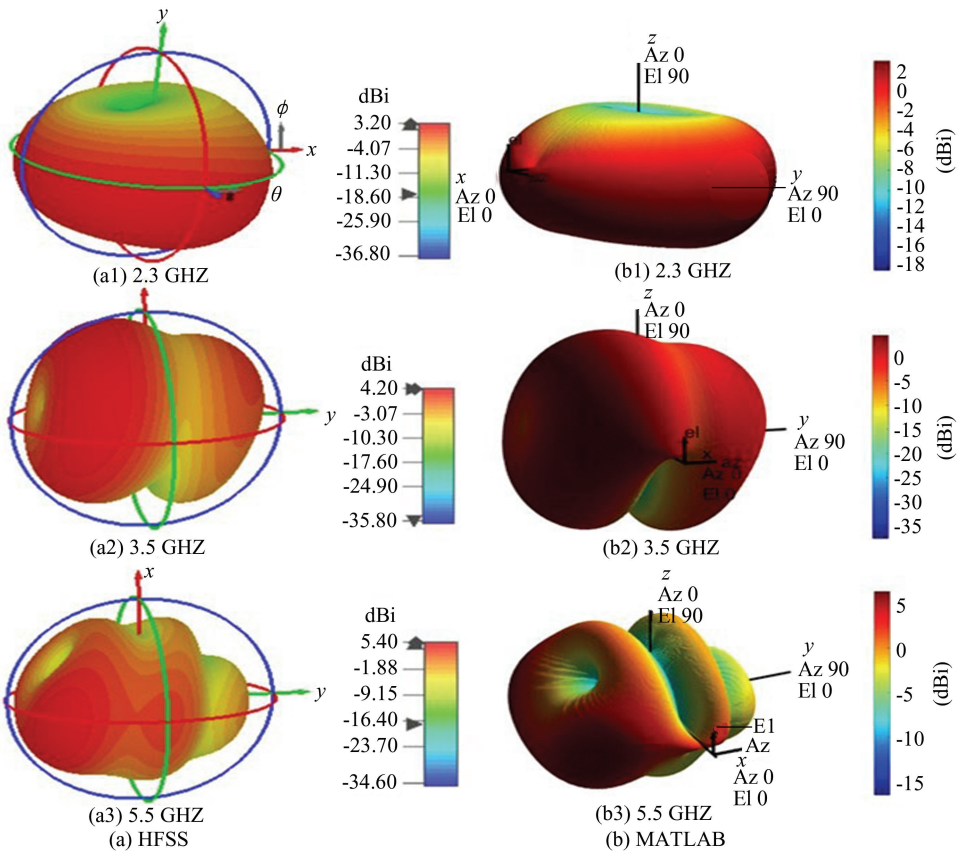

Fig.12 3D radiation patterns comparison of proposed antenna at 2.3, 3.5, and 5.5 GHz

Therefore, MATLAB-based simulations are carried out with 2 base stations, multiple transmitters, and receivers to resemble a use case for a smart street application using a 5G advanced communication network, as shown in Fig.13. In this proposed model, communication is performed across two layers. The first communication occurred between the two base stations with 8 transmitters placed at each light post in the street with a gap of 100 m each. In this communication, either LTE B40 or NR N41/N78 band is used. In the next step, communication occurs between the transmitters fixed to light posts (TR) and the user end device (UE) on the street via the 5th-generation Wi-Fi band. In this way, the proposed antenna is tested at both transmitters and user terminals to assess its feasibility for smart street applications.

As per the model, all these towers are first placed in MATLAB's inbuilt MAP based on their locations, and then a custom-replicated antenna is used at the Tx-Sites and UE terminals. The conventional antenna array is placed at the base stations with a transmitter power of 60 dB. The gain of the base station is shown in Fig.14 (a). Thereafter, all eight transmitters are placed at multiple locations on both sides of the street, with a usual height of 10 m and a receiver sensitivity of −90 dBm, as shown in Fig.14 (b).

After validating the radiation patterns at BS1 and BS2, the coverage of the same proposed antenna is observed in Fig.15 (a) with an array of 8×12. An antenna array is essential to provide high-quality coverage over a large area with beam-steering capabilities. For an efficient network, this capability of antenna arrays is essential to reduce energy loss from the antenna. It will track UE devices and orient the beam towards that direction, resulting in optimized beam steering. Thereafter, a communication network is established between the Tx-Sites with BS_1 and BS_2 shown in Fig.14 (b). It can be seen from the figure that a well coverage map link is established between the BS and Tx-Sites. The same custom antenna is then placed at all Tx-Sites, and their radiation patterns are depicted in Fig.15 (b). All these antennas will work as transmitters and receivers to communicate with both base stations and user terminals on the road.

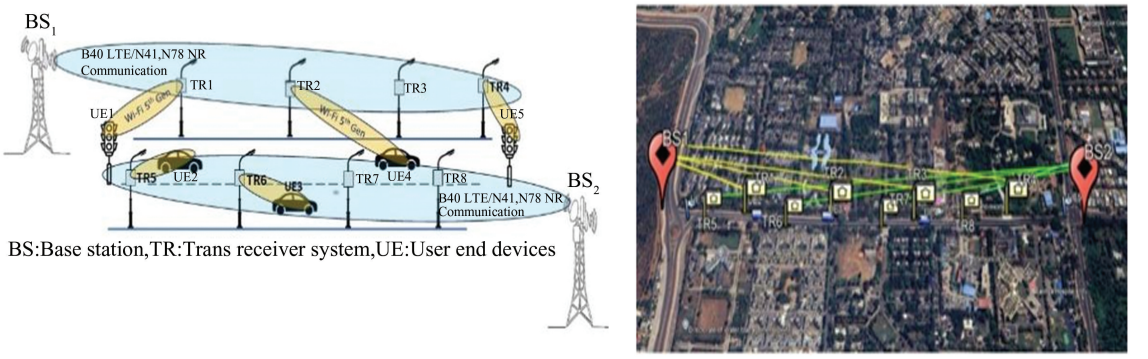

(a) Proposed model of base stations

(b) Tx- and Rx-sites and its satellite view

Fig.13 Proposed model of base stations ,and Tx- and Rx-Sites and its satellite view placed in a Map

(a) Single antenna radiation pattern placed at the base station

(b) Coverage map link among two base stations and eight Tx-sites

Fig.14 Single antenna radiation pattern placed at the base station, and coverage map link among two base stations and eight Tx-Sites

(a) Base station with 8×12 antenna array having 2 sectors at two different angles with a successful communication link to the Tx-sites

(b) Radiation pattern at all eight trans receivers with a single antenna at 5.5 GHz Wi-Fi communication

Fig.15 Base station with 8×12 antenna array having 2 sectors at two different angles with a successful communication link to the Tx-sites,and radiation pattern at all eight trans receivers with a single antenna at 5.5 GHz Wi-Fi communication

The proposed reconfigurable antenna is deployed at the transmitter side, and its performance is assessed based on the received signal strength at the receiver under various loss conditions such as rain, fog, and foliage. The received signal strengths for all eight Tx-Sites are presented in Table 6. A single reconfigurable antenna at the Tx-Site, the signal strength varies between −80 dB and −90 dB at the receivers. The path loss caused by 15 m of foliage is approximately 11 dB, while the combined loss due to 15 m of foliage and 10 mm rainfall occurring simultaneously is approximately 24 dB in the designed network. Due to

the combined effect of rain and foliage, the signal strength drops below −100 dB, and the receivers may experience call drops or data service interruptions. To avoid this call/data issue, a uniform rectangular array with the custom antenna as an element is installed at each base station. Further, the $\lambda/2$ spacing between individual elements, or between rows and columns, exhibits a gain of 17 dB for the designed communication network.

Table 6 Receiver signal strengths for various transmitters

Receiver name	Receiver signal strength (dB)					
	Free space		15 m foliage loss		15 m foliage and 10 mm rain	
	Single antenna	Antenna array	Single antenna	Antenna array	Single antenna	Antenna array
TR_1	−85.89	−76.67	−97.24	−88.02	−106.36	−97.14
TR_2	−87.66	−78.44	−99.01	−89.79	−108.13	−98.91
TR_3	−88.24	−79.02	−99.59	−90.37	−108.71	−99.49
TR_4	−89.43	−80.21	−100.78	−91.56	−109.90	−100.68
TR_5	−87.69	−78.47	−99.04	−89.82	−108.16	−98.94
TR_6	−83.74	−74.52	−95.09	−85.87	−104.21	−94.99
TR_7	−83.41	−74.19	−94.76	−85.54	−103.88	−94.66
TR_8	−86.04	−76.82	−97.39	−88.17	−106.51	−97.29

The received signal strength is now evaluated for all Txs with the same amount of foliage and rain path losses. The received signal strength is observed to be −70 dB to −80 dB under normal conditions, and it reduces to below −100 dB when both rain and foliage are present. With these signal strengths at the receivers, the communication will not face any call/data drop issues. Hence, these MATLAB simulations show that the proposed microstrip patch antenna and its array configuration may be used for a communication network in all types of atmospheric losses. This work develops a low-profile, planar, reconfigurable antenna integrated with a PIN diode, with frequency-tuning capability for the TDD B40, N41, N78 bands and the Wi-Fi 2C band. This ensures efficient spectrum utilization, compact integration into smart poles, and cost-effective deployment without multiple fixed antennas. The antenna is then tested in a smart street simulation environment created in MATLAB to ensure reliable performance and energy-efficient operation in the smart city communication structure.

4 Conclusions

A frequency- and polarization-tunable monopole antenna is designed using 5 PIN diodes for TDD B40, TDD NR N41, and N78 bands for 5G advanced communications. The antenna's performance is also verified across different atmospheric environments in MATLAB for advanced 5G applications, accounting for different path losses. Here, it is observed that the proposed antenna resonates at 2.3, 2.5, 3.5, and 5.5 GHz with various switching configurations, with received signal strengths ranging from −70 dB to −80 dB without any losses, and below −100 dB in the presence of rain and foliage combinedly. This demonstrates the viability of the presented 5G antenna for advanced outdoor smart street communications, given its compact size.

Conflict of interest:

The authors declare that they have no conflicts of interest.

References

[1] Paşalıoğlu H, Wang L, Bakır M, et al. A reconfigurable array and MIMO antenna for 18 GHz and 28/38 GHz applications. Measurement, 2025, 257(Part A): 118660. DOI: 10.1016/j.measurement.2025.118660.

[2] Boukarkar A, Lin X Q, Jiang Y, et al. Miniaturized single-feed multiband patch antennas. IEEE Transactions on Antennas and Propagation, 2016, 65(2): 850−854. DOI: 10.1109/TAP.2016.2632620.

[3] Motevasselian A, Whittow W G. Patch size reduction of rectangular microstrip antennas by means of a cuboid ridge. IET Microwaves, Antennas & Propagation, 2015, 9(15): 1727−1732. DOI: 10.1049/iet-map.2014.0559.

[4] Reddy V V, Sarma N V S N. Compact circularly polarized asymmetrical fractal boundary microstrip antenna for wireless applications. IEEE Antennas and Wireless Propagation Letters, 2014, 13: 118−121. DOI: 10.1109/

LAWP.2013.2296951.

[5] Oh J, Sarabandi K. A topology-based miniaturization of circularly polarized patch antennas. IEEE Transactions on Antennas and Propagation, 2013, 61(3): 1422-1426. DOI:10.1109/TAP.2012.2231915.

[6] Xu H X, Wang G M, Liang J G, et al. Compact circularly polarized antennas combining meta-surfaces and strong space-filling meta-resonators. IEEE Transactions on Antennas and Propagation, 2013, 61(7): 3442-3450. DOI:10.1109/TAP.2013.2255855.

[7] Dong Y, Toyao H, Itoh T. Design and characterization of miniaturized patch antennas loaded with complementary split-ring resonators. IEEE Transactions on Antennas and Propagation, 2012, 60(2): 772-785. DOI:10.1109/TAP.2011.2173120.

[8] Rajkumar R, Kiran K U. A metamaterial inspired compact open split ring resonator antenna for multiband operation. Wireless Personal Communications, 2017, 97(1): 951-965. DOI:10.1007/s11277-017-4545-0.

[9] Rajkumar R, Kommuri U K. A triangular complementary split ring resonator based compact metamaterial antenna for multiband operation. Wireless Personal Communications, 2018, 101(2): 1075-1089. DOI:10.1007/s11277-018-5749-7.

[10] Rajkumar R, Kommuri U K. A compact ACS-fed mirrored L-shaped monopole antenna with SRR loaded for multiband operation. Progress In Electromagnetics Research C, 2016, 64: 159-167. DOI: 10.2528/PIERC16031501.

[11] Venkatesan R, Rengasamy R, Naidu P V, et al. A compact meta-atom loaded asymmetric coplanar strip-fed monopole antenna for multiband operation. AEU-International Journal of Electronics and Communications, 2019, 98: 241-247. DOI:10.1016/j.aeue.2018.10.011.

[12] Kim C-S, Park J-S, Ahn D, et al. A novel 1-D periodic defected ground structure for planar circuits. IEEE Microwave and Guided Wave Letters, 2000, 10(4): 131-133. DOI:10.1109/75.846922.

[13] Yang M, Chen Z N, Lau P Y, et al. Miniaturized patch antenna with grounded strips. IEEE Transactions on Antennas and Propagation, 2015, 63(2): 843-848. DOI: 10.1109/TAP.2014.2382668.

[14] Pei J, Wang A G, Gao S, et al. Miniaturized triple-band antenna with a defected ground plane for WLAN/WiMAX applications. IEEE Antennas and Wireless Propagation Letters, 2011, 10: 298-301. DOI:10.1109/LAWP.2011.2140090.

[15] Lamsalli M, Hamichi A E, Boussouis A, et al. Genetic algorithm optimization for microstrip patch antenna miniaturization. Progress In Electromagnetics Research Letters, 2016, 60: 113-120. DOI: 10.2528/PIERL16041907.

[16] Li R L, Pan B, Laskar J, et al. A novel low-profile broadband dual-frequency planar antenna for wireless handsets. IEEE Transactions on Antennas and Propagation, 2008, 56(4): 1155-1162. DOI: 10.1109/TAP.2008.919171.

[17] Olawoye T O, Kumar P. A high gain antenna with DGS for sub-6 GHz 5G communications. Advanced Electromagnetics, 2022, 11(1): 41-50. DOI:10.7716/aem.v11i1.1670.

[18] Ajithra S, Maheswari A, Vidhusharani R, et al. Swastik slotted microstrip patch antenna for C band wireless applications. Tuijin Jishu/Journal of Propulsion Technology, 2024,45:1514-1520. DOI:10.52783/tjjpt.v45.i02.6071.

[19] Boutejdar A, Challal M, Mouhouche F, et al. Design and fabrication of a novel quadruple-band monopole antenna using a U-DGS and open-loop-ring resonators. Advanced Electromagnetics, 2017, 6(3): 59-63. DOI: 10.7716/aem.v6i3.573.

[20] El-Hakim H A, Mohamed H A. Engineering planar antenna using geometry arrangements for wireless communications and satellite applications. Scientific Reports, 2023, 13: Article number:19196. DOI:10.1038/s41598-023-46400-9.

[21] Hadri D E, Zugari A, Zakriti A, et al. Dual-band MIMO antenna with four CPW elements using polarization diversity for 5G mobile communication networks and satellite. Advanced Electromagnetics, 2023, 12(3): 43-53. DOI:10.7716/aem.v12i3.2077.

[22] Wang W, Fang Z, Tang K, et al. Wideband gain enhancement of MIMO antenna and its application in FMCW radar sensor integrated with CMOS-based transceiver chip for human respiratory monitoring. IEEE Transactions on Antennas and Propagation, 2023, 71(1): 318-329. DOI:10.1109/TAP.2022.3222802.

[23] Munir M E, Nasralla M M, Farman H. Design and development of super-compact millimeter wave antenna for future 5G vehicular applications. Proceedings of the 2024 IEEE 100th Vehicular Technology Conference (VTC2024-Fall). Piscataway: IEEE, 2024: 1-8. DOI: 10.1109/VTC2024-Fall63153.2024.10757480.

[24] Sethi W T, Kiani S H, Munir M E, et al. Pattern diversity based four-element dual-band MIMO patch antenna for 5G mmWave communication networks. Journal of Infrared, Millimeter, and Terahertz Waves, 2024, 45: 521-537. DOI:10.1007/s10762-024-00983-0.